nature astronomy

LETTERS

https://doi.org/10.1038/s41550-018-0668-9

A basal contribution from *p*-modes to the Alfvénic wave flux in the Sun's corona

R. J. Morton[1*], M. J. Weberg[1,2] and J. A. McLaughlin[1]

Many cool stars possess complex magnetic fields[1] that are considered to undertake a central role in the structuring and energizing of their atmospheres[2]. Alfvénic waves are thought to make a critical contribution to energy transfer along these magnetic fields, with the potential to heat plasma and accelerate stellar winds[3–5]. Despite Alfvénic waves having been identified in the Sun's atmosphere, the nature of the basal wave energy flux is poorly understood. It is generally assumed that the associated Poynting flux is generated solely in the photosphere and propagates into the corona, typically through the continuous buffeting of magnetic fields by turbulent convective cells[4,6,7]. Here, we provide evidence that the Sun's internal acoustic modes also contribute to the basal flux of Alfvénic waves, delivering a spatially ubiquitous input to the coronal energy balance that is sustained over the solar cycle. Alfvénic waves are thus a fundamental feature of the Sun's corona. Acknowledging that internal acoustic modes have a key role in injecting additional Poynting flux into the upper atmospheres of Sun-like stars has potentially significant consequences for the modelling of stellar coronae and winds.

Alfvénic fluctuations have been observed regularly in the solar wind since the 1970s[8,9] and are typically considered to be of solar origin. Their atmospheric counterpart was inferred from the non-thermal broadening of coronal emission lines[10], but only within the past two decades have studies of the Sun's atmosphere been able to demonstrate unambiguously that magnetized plasma structures undergo displacements transverse to the magnetic axis[11–13]. Here, we use infrared spectroscopic data (Fe XIII 1074.7 nm emission line) taken from the Coronal Multi-channel Polarimeter (CoMP) coronagraph, which yield Doppler velocity time-series above the limb in the Sun's corona and provide a measure of Alfvénic wave motions along a viewer's line of sight[14,15]. This is supported by extreme ultraviolet images of the corona from the 17.1 nm (Fe IX) channel on-board the Solar Dynamics Observatory (SDO) Atmospheric Imaging Assembly (AIA), which enables direct measurement of the transverse oscillatory displacements of the corona's fine-scale magnetic structure[16,17] (Fig. 1a–c). The datasets range between 2005 and 2015, hence covering various phases of the 11-year magnetic cycle, as the Sun's global magnetic geometry undergoes substantial changes (Supplementary Table 1). Since they can be subject to unambiguous and detailed measurements, we use the observed transverse displacements of magnetized plasma structures to probe the flux of Alfvénic wave energy.

The power spectral density (PSD) provides a means to investigate Alfvénic waves and is straightforward to obtain from CoMP Doppler velocity time-series (see Methods). The PSDs show evidence of power-law behaviour and display an enhancement of power around 4 mHz, sitting on the power-law baseline (Fig. 1d). This behaviour has been noted in previous observations of individual coronal regions[11,14]. Significantly, recent magnetohydrodynamic (MHD) wave models demonstrate the potential for coronal Alfvénic modes to be excited at the transition region[18–20], resulting from a double mode conversion of the Sun's internal acoustic pressure (*p*)-modes that have leaked into the atmosphere through magnetoacoustic portals[21]. It is the observed enhancement of power that is considered to be the signature of Alfvénic waves generated by *p*-modes[11,14,20]. However, if *p*-modes are to play a crucial role in exciting coronal Alfvénic waves, their signature should have a spatially ubiquitous presence throughout the corona and over the solar cycle. Through examination of the Alfvénic waves associated with the power enhancement, we demonstrate that this is indeed the case.

The counterpart to the velocity fluctuations measured by CoMP is thought to be the swaying motions of coronal structures observed in SDO/AIA[13,17], but no direct comparison has previously been undertaken. To remedy this, we measured large numbers of oscillatory Alfvénic waves in SDO/AIA (see Methods), where the imaging observations project the transient, transverse motions of plasma structures onto the plane of sky (Fig. 1b). The new detailed analysis of SDO/AIA data reveals that the coronal wave properties are more complex than was previously thought. A bivariate relationship is found between frequency and amplitude (Fig. 1c), with the periods and amplitudes occupying greater ranges of values than was previously reported[16,17]. The increased statistics permit a way to cross-calibrate the two sets of wave observations, enabling an estimate for the time-averaged wave properties of a particular coronal region and, hence, the PSD of the oscillatory motions in the SDO/AIA data (Fig. 1d).

The PSDs estimated from SDO/AIA data reveal that the power spectra have a parabolic profile, which peaks around 3–4 mHz. Other peaks are also visible above the parabolic profile, but with the current uncertainties we cannot say whether these are genuine (see Methods). Comparison between the CoMP and SDO/AIA estimates for the PSDs of the Alfvénic waves reveals that the frequency location of enhanced power is congruous to the peak of the parabolic profile. Furthermore, the spectral indices from power-law fits to both PSDs at frequencies >4 mHz are in excellent agreement. The close relationship between PSDs suggests that the enhanced power in the CoMP data is due to the transient, oscillatory motions observed in SDO/AIA.

Given this relationship, the enhanced power in the CoMP PSDs then provides a distinct marker for oscillatory Alfvénic waves and enables us to examine their nature throughout the corona and solar cycle. Our analysis of the CoMP data reveals that the enhancement exists in a large majority (>95%) of coronal power spectra, meaning that Alfvénic waves are present throughout the entire corona. An example of the key measured parameters obtained for 10 May 2014

[1]Department of Mathematics, Physics and Electrical Engineering, Northumbria University, Newcastle upon Tyne, UK. [2]Naval Research Laboratory, Washington, DC, USA. *e-mail: richard.morton@northumbria.ac.uk

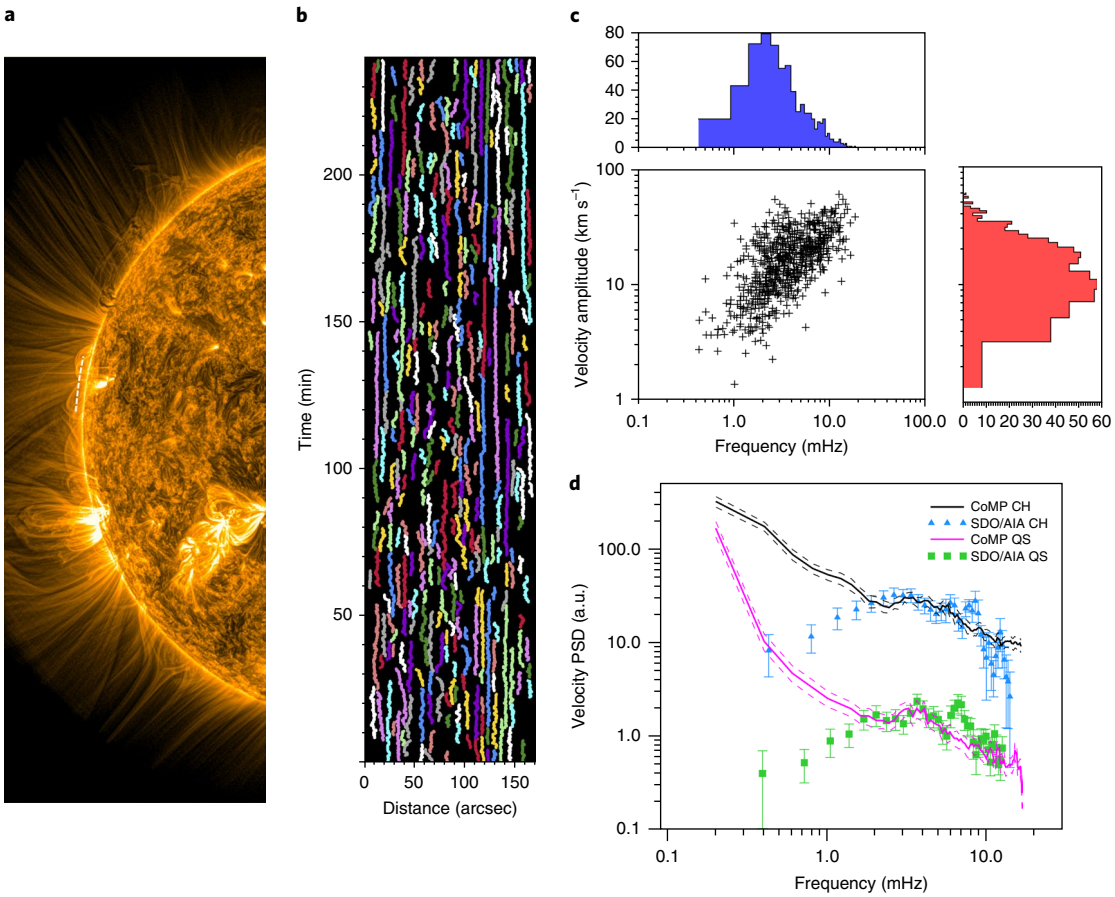

Fig. 1 | Signature of coronal Alfvénic waves. a, Data at the east limb from the SDO/AIA 17.1 nm channel reveal that the corona is comprised of fine-scale magnetic structures. **b**, Time–distance diagram using data from the quiet Sun (the region shown by a dashed line in **a**). The coloured tracks mark oscillating structures. Direct measurements of Alfvénic waves can be made through analysis of this diagram, with structures found to have displacements transverse to their axes. **c**, The measured properties of the waves are found to have a bivariate distribution, leading to approximately log-normal marginal distributions for both frequency (blue histogram) and amplitude (red histogram). **d**, Velocity PSD of Alfvénic waves from 27 March 2012, obtained from CoMP and SDO/AIA. The dashed lines and error bars represent s.e.m. These are typical examples of average spectra found in an open magnetic field region (coronal hole, CH) and the quiescent Sun (QS). The PSD is shown on an arbitrary scale as CoMP is known to underestimate the power due to coarse spatial resolution. The quiescent Sun data have also been offset by a factor of 1/10 for clarity.

data are shown in Fig. 2. We obtain similar findings when extending to data from different phases of the latest solar cycle (Figs. 3 and 4), from 2005 (two years before solar minimum) to the decline from maximum in 2015.

The frequency corresponding to the centre of the enhancement is found to fall within a narrow range, with its distribution having a mean and s.e.m. of 4.0 ± 0.1 mHz, and a s.d. of 1 mHz (Figs. 2 and 3a). While the sample populations are small for each yearly dataset, a comparison of the distributions from different years suggests that there is little variation in the centre values over the solar cycle. The enhanced power is distributed over a broader range of frequencies, and the characteristic width has a sharply peaked distribution around 0.12 frequency decades (Fig. 3b). The ubiquitous presence of the enhanced power through the corona is further evidenced in PSDs averaged across all of the coronal time-series from a single day (Fig. 4), where it is seen that the signature of Alfvénic waves is still clear.

Aside from the enhanced power, the coronal PSDs from CoMP also display ubiquitous power-law-like behaviour, which indicates the presence of stochastic (or non-oscillatory) Alfvénic waves (Fig. 1d). However, it should be kept in mind that we are examining a relatively short frequency range (0.1–10 mHz) and cannot determine whether the coronal Alfvénic waves display scale-free behaviour. Despite this shortcoming, we suggest that the index from the fitting of a power law to the coronal PSDs can also provide insight into the nature of the coronal velocity fluctuations. This is based on previous analysis[13] revealing that the Alfvénic waves in coronal holes had similar spectral slopes to those found from studies of Alfvénic fluctuations in fast solar wind streams (where the measurements span a much greater frequency range)[9]. The distribution of power-law indices shows a broad spread of values, with some evidence that it is bimodal (Fig. 3c). It is observed that the power-law index typically decreases as the complexity of the local magnetic field increases (Fig. 2b), in line with previous results[14]. In particular, open field regions were found to have the shallowest slopes (−1) and active regions the steepest (<−3/2). The distributions from the different stages of the solar cycle show qualitatively similar shapes and spread, although there is some indication of variability (Fig. 3c).

Alfvénic waves that propagate in the corona are expected to interact nonlinearly[4–6] and set up a turbulent MHD state[7,22]. The spectral indices for the inertial range of a fully turbulent MHD state are thought to be <−3/2 (see Supplementary Text Section 1 for further discussion on the expected scaling). If MHD turbulence is in action throughout the Sun's low corona, the results would suggest that, in general, the currently observable frequency ranges typically only reveal the energy-containing (or correlative) scales. Observations

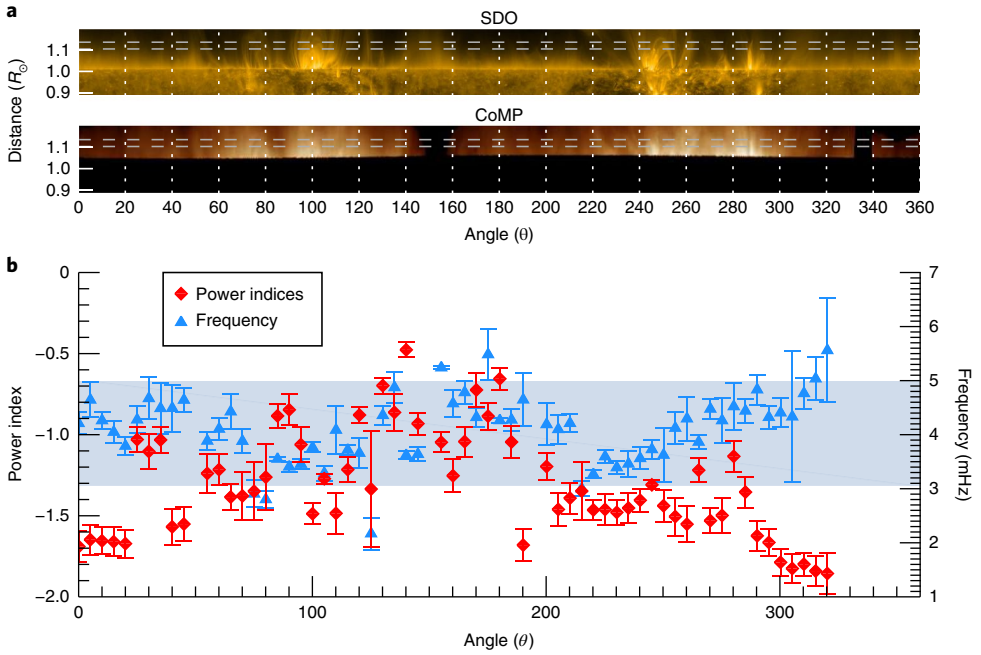

Fig. 2 | Properties of Alfvénic waves throughout the corona. a, Angle versus radius distance maps for SDO/AIA (top, 17.1 nm) and CoMP (bottom, 1,074.7 nm) showing intensity images of the corona on 10 May 2014 at 19:00 UT. The maps start at solar north and progress clockwise around the limb. The corona was split into 5°-wide segments and the CoMP data lying between the horizontal dashed grey lines were used to calculate the region-averaged Doppler velocity power spectra in each segment. The active regions visible are located at $\theta \approx 70°$ (AR12050), $\theta \approx 100°$ (AR12049) and $\theta \approx 250°$ (AR12061), and a coronal hole is present at $\theta \approx 150°$. It is found that the majority of Doppler velocity power spectra follow a power law with enhanced power around 4 mHz. **b**, The values of spectral indices (red diamonds) and frequency values for the centre of enhanced power (blue triangles) are shown from the nonlinear regression to the power spectra. Error bars represent s.e.m. The light blue shaded area highlights the 68% coverage of the central frequency probability density function (shown in Fig. 3a). The plot highlights that the centre of enhanced power is constrained to a narrow range of frequencies, while the spectral index shows variation as the structure of the magnetic field changes between open and closed geometries.

of Alfvénic fluctuations in the fast solar wind demonstrate that the slope of power spectra is a function of frequency[23], with a change from the energy-containing scales (index ≈−1) to the inertial scales around 5 mHz at 0.3 AU. The frequency of this break point decreases with distance from the Sun and is thought to be related to the decay of Alfvénic fluctuations with distance. With the presence of spectral indices close to −1 found in open and quiescent regions (Fig. 2 and refs. [13,14]), one may then naïvely expect such a break point to be located (if it exists) at higher frequencies in the lower corona. Hence, the current results imply that the onset of inertial scales in the corona occur generally at higher frequencies than those currently observable. However, the measured spectral indices suggest that approximately 25% of the coronal velocity fluctuations have indices <−3/2, found primarily in active regions (Fig. 2), which could indicate the development of turbulence cascades at observable frequencies in more complex magnetic geometries.

Overall, the properties of the oscillatory Alfvénic waves (for example, amplitude and frequencies) in the corona are unexpectedly similar throughout the solar cycle. Remarkably, the magnitude of the average coronal power enhancement varies only 10–15% between the dates analysed (Fig. 4a). The near-homogeneous nature of the global wave properties occurs despite the fact that they show variability across different magnetic geometries (Fig. 2; for example, the quiescent Sun compared with the active region). Moreover, at the peak of the enhancement, the extra power above the power-law component is comparable to that from the stochastic contribution (Fig. 4b). Hence, the results imply that the Sun's internal acoustic oscillations play a significant role in exciting Alfvénic wave modes at this frequency range, and signify that they provide a basal source of Poynting flux to the Sun's corona.

Recently, questions have been raised concerning the paradigm that a broad spectrum of coronal Alfvénic waves can originate from the photosphere. For example, the low ionization fraction of the photosphere potentially restricts Alfvénic wave excitation[24] and causes additional wave damping from ion-neutral collisions[25]. Additionally, the coupling of Alfvénic waves to slow magneto-acoustic waves via the ponderomotive force can also lead to significant wave damping in the chromosphere[26], while the transition region provides a substantial reflective barrier for their propagation into the corona[6]. The excitation of coronal Alfvénic modes at the transition region via the mode coupling (beginning with the Sun's internal acoustic waves) circumvents these issues. The findings presented here reveal that, despite concerns, a broad spectrum of Alfvénic waves is present throughout the Sun's corona, and distributions of wave properties change minimally over the solar cycle (Figs. 3 and 4a).

Importantly, a basal flux of Alfvénic waves is a crucial requirement for any mechanism to be considered as a major component in the heating of quiescent and open field regions in the Sun's atmosphere, where the temperature and emission measure are relatively homogeneous[27]. Using the wave measurements from SDO, an estimate for the observed Alfvénic wave energy flux in quiescent and coronal holes is 50–80 Wm^{-2} (see Supplementary Text Section 2), which falls below the standard values for coronal radiative losses (100–200 Wm^{-2}). However, the observed transverse motions are likely to be only a fractional detectable component of the total Alfvénic energy in the corona. Previous measurements of the transverse waves suggest a disparity between the observed wave amplitudes and those inferred from line widths[13,28], hinting at the presence of additional Alfvénic modes in the corona that cannot currently be directly measured. It is expected that *p*-modes can excite a number of Alfvénic modes[20]

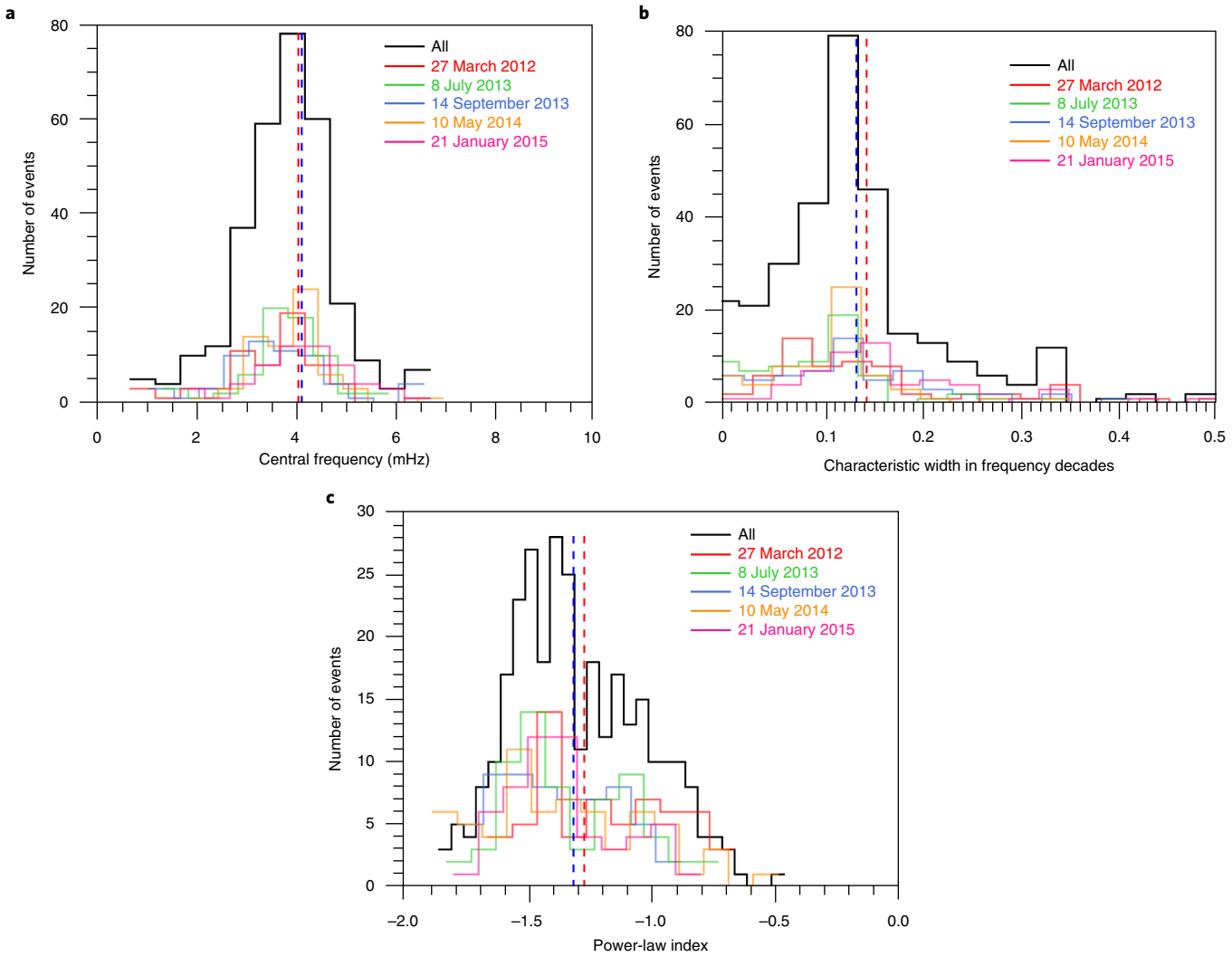

Fig. 3 | Power spectra parameter distributions for Alfvénic waves. The majority of coronal Doppler velocity power spectra are composed of a power law and a region of enhanced power (for example, Fig. 1d). The characteristic parameters of these features are determined from region-averaged power spectra and are subject to nonlinear regression. **a**, The frequency of the central location of the enhanced power shows a sharply peaked distribution (the central frequency of the log-normal function fit to the power spectra—parameter *D* in equation (6) in the Methods). **b**, Characteristic width of the log-normal function, showing that the enhanced power is found to be present over a broader frequency range. These distributions do not appear to vary significantly over the course of the solar cycle. **c**, The distribution of spectral indices from the coronal Doppler velocity power spectra shows a greater variability between years (for example, see the location of the left-hand peak). The variability could be related to the changes in coronal magnetic geometry over the solar cycle, reflecting the variation in the spectral index between the different geometries indicated in Fig. 2. However, we did not undertake further investigation to confirm this due to the small yearly sample sizes. A total of 305 measurements were taken from all dates (the parameters for individual measurements are given in Supplementary Table 2). The vertical red and blue dashed lines indicate the mean and median values, respectively.

and, if the non-thermal line widths are an accurate measure of the combined Alfvénic mode amplitudes[13,28], this implies that the energy requirements to counter radiative losses in the corona (excluding active regions) may easily be met by Alfvénic modes.

Furthermore, the findings may have significant implications for many Alfvénic wave models of solar plasma heating and wind acceleration[4–6] that largely neglect the additional energy contribution available from *p*-mode conversion in favour of excitation solely by the horizontal motions of the photospheric convection. Given that other cool, magnetized stars will have acoustic modes generated in their convective envelopes[29], *p*-modes potentially have an important role in energizing other stellar coronae as well.

Methods

Observations. The CoMP instrument[30] is able to take measurements of the Doppler shift of the Fe XIII emission line (1,074.7 nm), giving line-of-sight averaged velocities for the coronal plasma. The data are processed by the CoMP data pipeline, correcting for a number of standard data artefacts (for example, dark current, flat-fielding and subtraction of photospheric continuum emission). Final data products have a fixed cadence and spatial sampling of 4.46 arcsec. Specific details on the cadence and length of time-series are given in Supplementary Table 1. The data are rigidly aligned using cross-correlation to remove frame-to-frame misalignments. Most datasets contain measurements that cover the entire off-limb corona (excluding the darkest coronal holes), except 2005, which only covers one-quarter of the off-limb corona.

SDO/AIA[31] makes intensity measurements close to 17.1 nm using a relatively broad-band filter, of which a dominant contributor to emission in coronal plasma is Fe IX. The data are processed using the standard AIA data pipeline, with all datasets having a cadence of 12 s and a spatial sampling of 0.6 arcsec.

Wave nomenclature. Here, we use the term Alfvénic to refer to MHD wave modes that are highly incompressible, transverse, and for which the main restoring force is magnetic tension. Pure MHD modes only exist in idealized plasmas (that is, systems with an ignorable/invariant coordinate). For example, a homogeneous media can support Alfvén, slow and fast magneto-acoustic

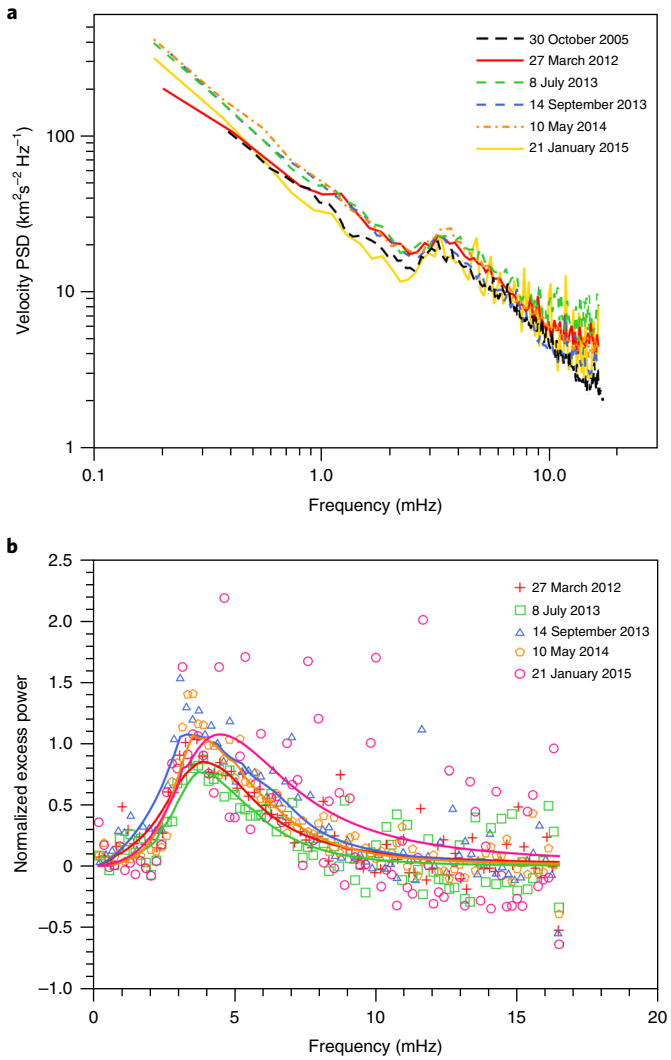

Fig. 4 | Global measures of Alfvénic waves through the solar cycle. a, Power spectra of velocity fluctuations after averaging over all of the eligible sections of the corona. The dates chosen cover the solar minimum in 2005, close to the northern (late 2011) and southern (late 2013) sunspot number maximum and the declining phase of the cycle. The enhancement of power around 4 mHz is clear in the global averages and across the solar cycle. **b**, On calculating the fraction of power above that of the underlying power law, the additional power at the peak of the enhancement is found to be comparable to the contribution from the stochastic velocity fluctuations. The data points are the average power spectra values, and the corresponding solid lines show the average values from the fitted models. Combined with the measured properties shown in Fig. 3, the results reveal that the enhanced power is largely insensitive to the variations in global magnetic geometry of the corona over the Sun's magnetic activity cycle.

modes[20], and a cylindrical flux tube model with a boundary discontinuity can support an infinite number of modes—a kink mode being one example. However, the solar atmosphere is an inhomogeneous, continuous and highly dynamic plasma where MHD wave modes have a hybrid nature. This property is highlighted by adding a simple continuous radial density profile to the cylindrical model[16,32,33], where the kink mode becomes strongly coupled to a quasi-torsional Alfvén mode[32] and will transfer energy to this other mode as it propagates; meaning that wave identification as kink or Alfvén is not absolute and is insufficient. While acknowledging that the observed transverse displacement of plasma structures observed in the CoMP and SDO/AIA data display characteristics of the idealized kink mode[15], the term Alfvénic better acknowledges the rich and complex nature of the coupled wave system within a real continuous and inhomogeneous media.

Automated wave detection. We have shown previously that the transverse modes in the corona can be directly measured with SDO/AIA, even in regions with a low signal-to-noise ratio[17,34]. These previous measurements were manual, meaning substantial time was required to collect a statistically significant number of samples, and the results were open to subjective event-selection biases. We now use an automated wave detection algorithm based on the Fourier analysis of time-series (Fig. 1b), which permits the collection of large samples of wave measurements. Due to the nature of the Fourier analysis, the algorithm is tuned to preferentially detect oscillatory signals.

The automated detection of waves in SDO/AIA data relies on using time–distance plots to measure the transverse displacements of the fine-scale magnetic structure projected on to the plane of sky. We use the NUWT software[34], which finds and measures the location of structures in the time–distance plots, generating times-series for the location of each structure. The latest version of the software enables an automated analysis of large data volumes, using fast Fourier transforms to measure the frequency and displacement amplitude of the swaying motions.

We note that the SDO data possess an inherent limitation for measuring the waves, due to the instrument resolution. Potentially, this could alter the shape (and trend) of the bivariate distribution found in the measurements depicted in Fig. 1c. The higher-frequency, oscillatory, transverse waves found typically have the smallest displacement amplitudes (although they have the largest velocity amplitudes); hence, there is the potential that high-frequency, small-displacement amplitude waves are excluded from our measurements (that is, waves occupying the lower right-hand part of the frequency–velocity amplitude plot in Fig. 1c). However, we believe that this is not the case. If we were to assume that there are unseen high-frequency waves with smaller displacement/velocity amplitudes, this would lead to smaller values of time-averaged power. Hence, the corresponding PSD will also be altered (Fig. 1d), and it would have smaller power at higher frequencies than those currently shown. Such a shift in the high-frequency power would then lead to an inconsistency between the CoMP and SDO PSDs, which is not observed to be the case.

PSD. The CoMP PSDs used in the analysis are based on region-averaged PSDs, increasing the signal-to-noise ratio over individual estimates of the PSD. The corona is divided into 5° sections, with each section containing between 130 and 200 individual time-series. The division starts at solar north. The choice of location of the section boundaries is arbitrary, in the sense that the corona is equally divided up without consideration of the magnetic geometry. We work under the assumption that in each section of the corona, the time-series are all different realizations of the same process. Certain sections of the corona are removed from the analysis where there is no signal or only a very small number of time-series. The periodogram is a common way to display the time-averaged power as a function of the frequency and is easily obtained from the discrete Fourier transform of an evenly sampled velocity time-series of length N samples, evaluated at discrete frequencies, $f_j = j/(Ndt)$ for $j = 1,..,N/2$ (where dt is the cadence).

It is known that the power of the discrete Fourier transform in each frequency bin is distributed as χ^2 with 2 d.f.[35]; hence, the mean log-power at each frequency ordinate is calculated in each section and a bias correction is applied. The distribution of the mean log-power at each frequency ordinate is checked for normality by generating bootstrap samples of the mean log-power from the sample distributions. The distributions of the bootstrap mean are compared with a normal distribution using a Kolmogorov–Smirnov test at the 5% level (correcting for unknown mean and variance, and also for multiple comparisons). It is found that the majority (>99.9%) of the bootstrap distributions show no evidence of differing from a normal distribution at this level. From the distribution of bootstrap means, the s.d. of the mean is measured for each frequency ordinate. A correction is applied to the s.d. values of the means to account for the dependence of time-series from neighbouring pixels in the data[36].

The calculation of the PSD for SDO/AIA data is different from that for CoMP. The time-series generated by NUWT are of varying length, so cannot be combined without correction. The Fourier power is directly comparable to the mean-square velocity. Assuming each signal measured, V, is a sinusoid, it exists for a fixed time T over the course of the observation period, Ndt; for example:

$$V = \begin{cases} A\sin(\omega t) & 0 < t \leq T \\ 0 & T < t \leq Ndt \end{cases} \quad (1)$$

The mean-squared velocity for each sinusoid is then:

$$\langle v_{sin}^2 \rangle = \frac{1}{T} \sum_0^T V^2 \quad (2)$$

Over the total observation period, the mean-squared velocity is:

$$\langle v_i^2 \rangle = \frac{T}{Ndt} \langle v_{\sin}^2 \rangle \quad (3)$$

for each signal. For a fixed frequency, there may be a number, P, of independent signals measured over the total time, of differing length T_1, T_2,.... The total

mean-square velocity is just an addition of the mean-square velocity of each signal. For simplicity, if we assume that each signal has a characteristic time T and amplitude, the total mean-square velocity is given by:

$$\langle v_{\rm tot}^2 \rangle = \frac{PT}{Ndt} \langle v_{\rm sin}^2 \rangle \quad (4)$$

To calculate the actual total mean-square velocity, an estimate of the occurrence rate of the waves over the total observation period at a fixed frequency is required. To obtain this, we bin the measured signals as a function of the frequency (that is, the histogram in Fig. 1b), denoting the number of signals in each bin as P. Finally, each value is normalized by the total number of signals observed, $P_{\rm tot}$, due to the time–distance diagrams spanning a large spatial extent. Mean-square velocities of signals that fall within each frequency bin are multiplied by the respective $P/P_{\rm tot}$.

To obtain the average PSD from the individual values, non-parametric regression is performed using a Nadaraya–Watson kernel estimator. This methodology uses multivariate kernel density estimation as an alternative to histograms[37]. The kernel bandwidth is selected by cross-validation, and bootstrapping is used to determine the s.e.m. values (see Supplementary Text Section 3).

The lower number of measurements for waves with frequencies greater than ~4 mHz (Fig. 1c) means that the significance of peaks above the parabolic shape is small. We note that the SDO/AIA PSD is limited to a smaller range of frequencies than that from CoMP, which is mainly determined by the lifetimes of the features under observation (for example, plumes, coronal loops and so on). The visibility of the coronal features is potentially due to the thermodynamic cycle of the atmospheric plasma, which is thought to be subject to impulsive or episodic heating and cooling events[38]. This would impact on the low-frequency part of the PSD (<0.8 mHz), potentially leading to an underestimate of the power here. Furthermore, Fig. 1c demonstrates that the wave velocity amplitude increases with the frequency, suggesting that the higher-frequency Alfvénic waves typically carry more energy than their lower-frequency counterparts. We do not believe that this feature is an artefact of our methodology, as testing of the sensitivity suggests we should be able to measure smaller disturbances. Moreover, the occurrence of high-frequency waves is sporadic in comparison; hence, they contribute less energy on average, which is reflected in the PSD from both instruments. Any unresolved high-frequency waves with velocity amplitudes smaller than those shown would decrease the PSD at high frequencies and lead to disagreement with the CoMP data. The observed bivariate behaviour explains, in part, the approximate log-normal marginal distributions of the wave properties observed previously[17].

Nonlinear regression and model comparison. We perform nonlinear regression on the mean log-power spectra in each section of the corona. Two models are used for regression, to assess whether all power spectra studied display the enhancement that peaks around 4 mHz, and to parametrize the properties of the enhancement. We start with the hypothesis that all power spectra display power-law behaviour, and some of these may have a power enhancement. The first model (M1) we fit to the data is a simple power law; namely:

$$P_{\rm M1}(f_j) = Af_j^{\alpha} + B \quad (5)$$

where α is the power-law index, A is a constant of proportionality and B is a constant to describe the noise-dominated power ordinates at high frequencies (that is, B represents a Gaussian white noise process). The second model (M2) takes into account any excess power that causes a deviation from power-law behaviour via the addition of an exponential term:

$$P_{\rm M2}(f_j) = Af_j^{\alpha} + B + C\exp\left(-\frac{(\ln f_j - D)^2}{2E^2}\right) \quad (6)$$

where the constants C, D and E parametrize a log-normal function.

To fit the models to the data, we use maximum likelihood, maximizing:

$$L = \prod_{j=1}^{N/2-1} (2\pi\sigma_j^2)^{-1/2} \exp\left(-\frac{(P_j - P_M(f_j))^2}{\sigma_j^2}\right) \quad (7)$$

for normally distributed data (neglecting the power at the Nyquist frequency), fitting the models in log-space (see Supplementary Text Section 3). Supplementary Table 2 provides the details of the parameters obtained from the fitting of the model given in equation (6).

To compare the model's ability to describe the power spectra, we use the Akaike information criterion (AIC). The AIC is based on information theory and provides a means to measure the information lost when fitting a model, enabling a comparison between the goodness of fit and model complexity. The measure of the AIC is defined as:

$$\mathrm{AIC} = 2k - 2\ln(L_{\rm max}) + \frac{2k(k+1)}{n-k-1} \quad (8)$$

where $L_{\rm max}$ is the maximum value of the likelihood surface, k is the number of parameters and n is the sample size. The model comparison is summarized by the quantity $\Delta_{\rm AIC} = \mathrm{AIC}_{\rm M1} - \mathrm{AIC}_{\rm M2}$. The suitability of the $\Delta_{\rm AIC}$ statistic for comparison between these two models is tested by performing Monte Carlo simulations. The simulations mimic the described analysis procedure, using time-series generated from the suggested models (see Supplementary Text Section 3) and run 5,000 times. When using M2 as the underlying power model, the simulations demonstrate that approximately 95% of the time-model M2 is favoured correctly. In contrast, on performing simulations using only a power-law spectra (M1), it is found that the AIC test performs worse, identifying M1 power spectra only 70% of the time. The observed percentage of M2-type models preferred by the AIC test is in line with the expected rate of success from the Monte Carlo simulations, which would imply that all measured coronal power spectra contain a power enhancement. Moreover, if we are expecting to identify ~70% of the M1-type spectra from the AIC test, this further supports the idea that the potential number of M1-type power spectra in the corona is small.

Data availability

The data that support the findings of this study are available from the corresponding author upon reasonable request. The SDO data are available from the Joint Science Operations Center (http://jsoc.stanford.edu). The CoMP data are available from the High Altitude Observatory data repository (https://www2.hao.ucar.edu/mlso/mlso-home-page).

Received: 28 February 2018; Accepted: 29 November 2018;
Published online: 28 January 2019

References

1. Reiners, A. Observations of cool-star magnetic fields. *Living Rev. Sol. Phys.* **9**, 1 (2012).
2. Testa, P., Saar, S. H. & Drake, J. J. Stellar activity and coronal heating: an overview of recent results. *Phil. Trans. R. Soc. A* **373**, 20140259 (2015).
3. Narain, U. & Ulmschneider, P. Chromospheric and coronal heating mechanisms II. *Space Sci. Rev.* **75**, 453–509 (1996).
4. Suzuki, T. K. & Inutsuka, S. Making the corona and the fast solar wind: a self-consistent simulation for the low-frequency Alfvén waves from the photosphere to 0.3au. *Astrophys. J.* **632**, L49–L52 (2005).
5. Verdini, A. & Velli, M. Alfvén waves and turbulence in the solar atmosphere and solar wind. *Astrophys. J.* **662**, 669–676 (2007).
6. Cranmer, S. R. & van Ballegooijen, A. A. On the generation, propagation, and reflection of Alfvén waves from the solar photosphere to the distant heliosphere. *Astrophys. J. Suppl. Ser.* **156**, 265–293 (2005).
7. Van Ballegooijen, A. A., Asgari-Targhi, M., Cranmer, S. R. & DeLuca, E. E. Heating of the solar chromosphere and corona by Alfvén wave turbulence. *Astrophys. J.* **736**, 3 (2011).
8. Belcher, J. W. & Davis, L. J. Large-amplitude Alfvén waves in the interplanetary medium 2. *J. Geophys. Res.* **76**, 3534–3563 (1971).
9. Bruno, R. & Carbone, V. The solar wind as a turbulence laboratory. *Living Rev. Sol. Phys.* **2**, 4 (2005).
10. Banerjee, D., Teriaca, L., Doyle, J. G. & Wilhelm, K. Broadening of SI VIII lines observed in the solar polar coronal holes. *Astron. Astrophys.* **339**, 208–214 (1998).
11. Tomczyk, S. et al. Alfvén waves in the solar corona. *Science* **317**, 1192–1196 (2007).
12. De Pontieu, B. et al. Chromospheric Alfvénic waves strong enough to power the solar wind. *Science* **318**, 1574–1577 (2007).
13. Morton, R. J., Tomczyk, S. & Pinto, R. F. Investigating Alfvénic wave propagation in coronal open-field regions. *Nat. Commun.* **6**, 7813 (2015).
14. Morton, R. J., Tomczyk, S. & Pinto, R. F. A global view of velocity fluctuations in the corona below 1.3 $R_{\odot}$ with CoMP. *Astrophys. J.* **828**, 89 (2016).
15. Van Doorsselaere, T., Nakariakov, V. M. & Verwichte, E. Detection of waves in the solar corona: kink or Alfvén? *Astrophys. J. Lett.* **676**, L73 (2008).
16. McIntosh, S. W. et al. Alfvénic waves with sufficient energy to power the quiet solar corona and fast solar wind. *Nature* **475**, 447–480 (2011).
17. Thurgood, J. O., Morton, R. J. & McLaughlin, J. A. First direct measurements of transverse waves in solar polar plumes using SDO/AIA. *Astrophys. J.* **790**, L2 (2014).
18. Cally, P. S. & Goossens, M. Three-dimensional MHD wave propagation and conversion to Alfvén waves near the solar surface. I. Direct numerical solution. *Sol. Phys.* **251**, 251–265 (2008).
19. Cally, P. S. & Hansen, S. C. Benchmarking fast-to-Alfvén mode conversion in a cold magnetohydrodynamic plasma. *Astrophys. J.* **738**, 119 (2011).
20. Cally, P. S. Alfvén waves in the structured solar corona. *Mon. Not. R. Astron. Soc.* **466**, 413–424 (2017).
21. Jefferies, S. M. et al. Magnetoacoustic portals and the basal heating of the solar chromosphere. *Astrophys. J.* **648**, L151–L155 (2006).

22. Matthaeus, W. H., Zank, G. P., Oughton, S., Mullan, D. J. & Dmitruk, P. Coronal heating by magnetohydrodynamic turbulence driven by reflected low-frequency waves. *Astrophys. J.* **523**, L93–L96 (1999).
23. Bavassano, B., Dobrowolny, M., Mariani, F. & Ness, N. F. Radial evolution of power spectra of interplanetary Alfvénic turbulence. *J. Geophys. Res.* **87**, 3617–3622 (1982).
24. Pandey, B. P., Vranjes, J. & Krishan, V. Waves in the solar photosphere. *Mon. Not. R. Astron. Soc.* **386**, 1635–1643 (2008).
25. Soler, R., Ballester, J. L. & Zaqarashvili, T. V. Overdamped Alfvén waves due to ion-neutral collisions in the solar chromosphere. *Astron. Astrophys.* **573**, 79 (2015).
26. Arber, T. D., Brady, C. S. & Shelyag, S. Alfvén wave heating of the solar chromosphere: 1.5D models. *Astrophys. J.* **817**, 94 (2016).
27. Morgan, H. & Taroyan, Y. Global conditions in the solar corona from 2010 to 2017. *Sci. Adv.* **3**, e1602056 (2017).
28. McIntosh, S. W. & De Pontieu, B. Estimating the "dark" energy content of the solar corona. *Astrophys. J.* **761**, 138 (2012).
29. Chaplin, W. J. & Miglio, A. Asteroseismology of solar-type and red-giant stars. *Annu. Rev. Astron. Astrophys.* **51**, 353–392 (2013).
30. Tomczyk, S. et al. An instrument to measure coronal emission line polarization. *Sol. Phys.* **247**, 411–428 (2008).
31. Lemen, J. R. et al. The Atmospheric Imaging Assembly (AIA) on the Solar Dynamics Observatory (SDO). *Sol. Phys.* **275**, 17–40 (2012).
32. Goossens, M., Terradas, J., Andries, J., Arregui, I. & Ballester, J. L. On the nature of kink MHD waves in magnetic flux tubes. *Astron. Astrophys.* **503**, 213–223 (2009).
33. Goossens, M. et al. Surface Alfvén waves in solar flux tubes. *Astrophys. J.* **753**, 111 (2012).
34. Weberg, M., Morton, R. J. & McLaughlin, J. A. An automated algorithm for identifying and tracking transverse waves in solar images. *Astrophys. J.* **852**, 57 (2018).
35. Vaughan, S. A simple test for periodic signals in red noise. *Astron. Astrophys.* **431**, 391–403 (2005).
36. Ireland, J., McAteer, R. T. J. & Inglis, A. R. Coronal Fourier power spectra: implications for coronal seismology and coronal heating. *Astrophys. J.* **798**, 12 (2015).
37. Feigelson, E. & Babu, G. J. *Modern Statistical Methods for Astronomy* (Cambridge Univ. Press, Cambridge, 2012).
38. De Pontieu, B. et al. The origins of hot plasma in the solar corona. *Science* **331**, 55–58 (2011).

Acknowledgements

All authors acknowledge that this material is based on work supported by the Air Force Office of Scientific Research, Air Force Material Command, USAF under award number FA9550-16-1-0032, and the Science and Technology Facilities Council via grant number ST/L006243/1. R.J.M. is grateful to the Leverhulme Trust for the award of an Early Career Fellowship, and the High Altitude Observatory for financial assistance. M.J.W. acknowledges additional support from NASA grant NNH16AC39I and basic research funds from the Chief of Naval Research. R.J.M. is also grateful for discussions at ISSI, Bern (*Towards Dynamic Solar Atmospheric Magneto-Seismology with New Generation Instrumentation*) and with G. Li and S. Tomczyk. The authors acknowledge the work of the NASA/SDO and AIA science teams, and National Center for Atmospheric Research/High Altitude Observatory CoMP instrument team.

Author contributions

R.J.M. performed the analysis of the CoMP data. R.J.M., M.J.W. and J.A.M. performed the analysis of the SDO data. All authors discussed the results and contributed to the writing of the manuscript.

Competing interests

The authors declare no competing interests.

Additional information

Supplementary information is available for this paper at https://doi.org/10.1038/s41550-018-0668-9.

Reprints and permissions information is available at www.nature.com/reprints.

Correspondence and requests for materials should be addressed to R.J.M.

Publisher's note: Springer Nature remains neutral with regard to jurisdictional claims in published maps and institutional affiliations.